Journal Name

RSCPublishing

ARTICLE

The synthesis and characterisation of coordination and hydrogen-bonded networks based on 4-(3,5-dimethyl-1*H*-pyrazol-4-yl)benzoic acid

Cite this: DOI: 10.1039/x0xx00000x

Received 00th January 2012,
Accepted 00th January 2012

DOI: 10.1039/x0xx00000x

www.rsc.org/

Macguire R. Bryant,[a] Andrew D. Burrrows,*[b] Christopher M. Fitchett,[c] Chris S. Hawes,[c] Sally O. Hunter,[a] Luke L. Keenan,[b] David J. Kelly,[b] Paul E. Kruger,*[c,d] Mary F. Mahon,[b] and Christopher Richardson*[a]

The synthesis, structural and thermal characterisation of a number of coordination complexes featuring the *N,O*-heteroditopic ligand 4-(3,5-dimethyl-1*H*-pyrazol-4-yl)benzoate, H**L** are reported. The reaction of H_2**L** with cobalt(II) and nickel(II) nitrates at room temperature in basic DMF/H_2O solution gave discrete mononuclear coordination complexes with the general formula $[M(H\mathbf{L})_2(H_2O)_4]\cdot 2DMF$ (M = Co (**1**), Ni (**2**)), whereas the reaction with zinc(II) nitrate gave $[Zn(\mathbf{HL})_2]_\infty$, **3**, a coordination polymer with distorted diamondoid topology and fourfold interpenetration. Coordination about the tetrahedral Zn(II) nodes in **3** are furnished by two pyrazolyl nitrogen atoms and two carboxylate oxygen atoms to give a mixed N_2O_2 donor set. Isotopological coordination polymers of zinc(II), $\{[Zn(H\mathbf{L})_2]\cdot 2CH_3OH\cdot H_2O\}_\infty$, **4**, and cobalt(II), $[Co(H\mathbf{L})_2]_\infty$, **5**, are formed when the reactions are carried out under solvothermal conditions in methanol (80 °C) and water (180 °C), respectively. The reaction of **H_2L** with cadmium(II) nitrate at room temperature in methanol gives $\{[Cd(H\mathbf{L})_2(MeOH)_2]\cdot 1.8MeOH\}_\infty$ **6**, a 2-D (4,4)-connected coordination polymer, whereas with copper(II) the formation of green crystals that transform into purple crystals is observed. The metastable green phase $[Cu_3(H\mathbf{L})_4(\mu_2\text{-}SO_4)(H_2O)_3]_\infty$, **7**, crystallises with conserved binding domains of the heteroditopic ligand and contains two different metal nodes: a dicopper carboxylate paddle wheel motif, and, a dicopper unit bridged by sulfate ions and coordinated by ligand pyrazolyl nitrogen atoms. The resultant purple phase $\{[Cu(H\mathbf{L})_2]\cdot 4CH_3OH\cdot H_2O\}_\infty$, **8**, however, has single copper ion nodes coordinated by mixed N_2O_2 donor sets with *trans*-square planar geometry and is fourfold interpenetrated. The desolvation of **8** was followed by powder X-ray diffraction and single crystal X-ray diffraction which show desolvation induces the transition to a more closely packed structure while the coordination geometry about the copper ions and the network topology is retained. Powder X-ray diffraction and microanalysis were used to characterise the bulk purity of the coordination materials **1–6** and **8**. The thermal characteristics of **1–2, 4–6** and **8** were studied by TG-DTA. This led to the curious observation of small exothermic events in networks **4**, **6**, and **8** that appear to be linked to their decomposition. In addition, the solid state structures of H_2**L** and that of its protonated salt, **H_2L**·HNO_3, were also determined and revealed that H_2**L** forms a 2-D hydrogen bonded polymer incorporating helical chains formed through N-H···O and O-H···N interactions, and that $[H_3\mathbf{L}]NO_3$ forms a 1-D hydrogen-bonded polymer.

Introduction

The construction of coordination networks *by design* is a topic of continuing high interest.[1] with this interest stemming from the potential of these materials in applications ranging from optoelectronics to catalysis.[2] A challenge in the field is to create coordination networks with more than one functional unit, which increases the complexity of the framework. One way of achieving such complexity is through the structure of the bridging ligand component.[3] In this regard, heteroditopic ligands offer the prospect of constructing complex coordination networks, with each end of the linker coordinating to a different type of metal node (also known as Secondary Building Units or SBUs). There is also the potential for the metal nodes in these structures to contain both types of donor atom or to have nodes with conserved binding domains where all the coordinating

atoms are of one type. By designing ligands with binding domains that are different in nature, it is possible that coordination networks can be made that exploit "soft-soft" and "hard-hard" coordination interactions.

We are interested in ditopic and heteroditopic molecules featuring pyrazole units as ligands for constructing coordination networks, and have worked with pyrazole-pyridines,[4, 5] indazole-carboxylates[6, 7] and pyrazole-carboxylates.[8] Pyrazole ligands are an attractive option for a number of reasons. As commented on by Long and collaborators[9, 10] the deprotonation of pyrazoles and the binding of the resulting pyrazolates confers good thermal and chemical stability in coordination networks. Indeed, Navarro and co-workers have explored stable bis-pyrazolate[11-13] and pyrazolate-carboxylate[14, 15] networks for sequestration-type applications. The pyrazole ring can also coordinate in a neutral form. This mode of bonding offers additional hydrogen bonding capacity and we reasoned that this offers a mechanism for secondary organisation of the supramolecular structure of the coordination materials.

4-(3,5-Dimethyl-1*H*-pyrazol-4-yl)benzoic acid (H_2**L**) is heteroditopic with the potential to bridge metal centres in a number of ways through pyrazolyl nitrogen and carboxylate oxygen atoms and also in anionic (H**L**$^-$) or dianionic forms (**L**$^{2-}$) (Figure 1).

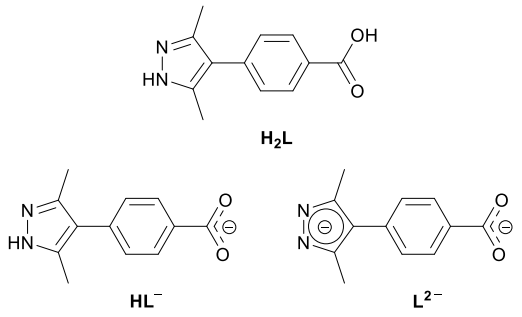

Figure 1. The structure of H_2**L** and of its anionic counterparts, H**L**$^-$ and **L**$^{2-}$

Despite these attractive features, H_2**L** has only been used in a few reports. Janiak and co-workers formed a structure isoreticular to MOF-5 where dianionic **L**$^{2-}$ units bridge Zn_4O nodes.[16] Zhang *et. al.* have reported different forms of zinc coordination networks where the anionic H**L**$^-$ bridges zinc ions, and studied solid phase micro extraction[17] and the topological subtlety of the materials.[18] The porous zinc coordination network MAF-X8 has been further examined for *p*-xylene separation capability *in silico*.[19] A beautiful example of hard-hard soft-soft interactions dictating structure formation has been reported by Zhou and co-workers.[20] The reaction of H_2**L** with copper(II) led to a structure containing conserved binding domains featuring well-known pyrazolate-bridged trigonal copper(I) units [Cu_3(pyrazolate)$_3$] from *in situ* reduction of the copper(II) ions, and square carboxylate-bridged copper(II) paddlewheels in a coordination network of Pt_3O_4 topology.[20] The versatility and potential of the pyrazole-benzoate synthon is also seen by the incorporation into methylene 'hinged' bispyrazole-benzoate ligands to successfully target flexible MOFs.[21, 22]

In this paper we report the structures of H_2**L** and its nitrate salt and describe the syntheses, structures and thermal studies of coordination networks and hydrogen-bonded networks of metal complexes of H**L**$^-$.

Experimental

General

Unless otherwise specified, all reagents and starting materials were of reagent grade or better and purchased from standard suppliers and used as received. Water was purified by reverse osmosis. Where anhydrous solvents were required, HPLC-grade solvent was either distilled from standard drying agents or dried by passing over a sealed column of activated alumina.

Powder X-ray diffraction patterns were obtained using a GBC-MMA diffractometer operating at 1.0 kW with samples mounted on 1" quartz substrates. Simultaneous thermo-gravimetric-differential thermal analysis (TG-DTA) traces were obtained using a Shimadzu DTG-60 instrument fitted with a FC-60A flow rate controller and TA-60WS thermal analyser using measuring parameters of 10 °C per min under nitrogen flow of 20 cm^3min^{-1}. Infrared spectra were obtained using a Shimadzu IR Affinity-1 FTIR, fitted with a MIRacle 10 single reflection ATR accessory. Microanalyses were recorded by Mr Alan Carver (University of Bath Microanalysis Service) or Gillian Maxwell (University College London Microanalysis Service) or the Microanalytical Unit, Australian National University, Australia or the Campbell Microanalytical Laboratory, University of Otago, New Zealand.

X-ray crystallography

X-ray crystallographic data collection at the University of Canterbury was carried out with an Oxford-Agilent SuperNova instrument with focused microsource Cu-Kα radiation (λ = 1.5418 Å) radiation and ATLAS CCD area detector. Single crystals were analysed at the University of Bath using a Nonius Kappa CCD diffractometer and Mo-Kα radiation (λ = 0.71073 Å) and CCD area detector. The diffraction data for compounds **7** and **8**-*dry* were collected at the MX1 beamline on the Australian Synchrotron, Victoria, Australia, operating at 17.4 keV (λ = 0.7108) with data collections conducted using BluIce control software.[23] These datasets were processed using the XDS software suite,[24] with anomalous dispersion corrections for the non-standard wavelength applied using Brennan and Cowan data.[25] All structures were solved using direct methods with SHELXS[26] and refined on F^2 using all data by full matrix least-squares procedures with SHELXL-97[27] within OLEX-2[28] or through the X-Seed interface.[29] Unless otherwise noted, non-hydrogen atoms were refined with anisotropic displacement parameters. Unless otherwise noted, hydrogen atoms were included in calculated positions with isotropic displacement parameters either 1.2 times or 1.5 times the isotropic equivalent of their carrier atoms, where appropriate, with the exception of

selected hydrogen bonding sites, in which the hydrogen atoms were manually located from residual Fourier peaks and modelled with appropriate bond length restraints and U_{iso} dependences. The functions minimized were $\sum w(F_o^2 - F_c^2)$, with $w = [\sigma^2(F_o^2) + aP^2 + bP]^{-1}$, where $P = [\max(F_o)^2 + 2F_c^2]/3$.

Synthesis of H_2L

The synthesis of H_2**L** has been reported previously.[30] We prepared H_2**L** using routes that enabled a final step of ester hydrolysis and the synthetic details are provided in the ESI.

General method for the preparation of {[Co(HL)$_2$(H$_2$O)$_4$]·2DMF}, 1; {[Co(HL)$_2$(H$_2$O)$_4$]·2DMF}, 2; and [Zn(HL)$_2$]∞, 3

A solution of H_2**L** (22.7 mg, 0.10 mmol) in DMF (1.25 mL) and 1.0 M NaOH (100 μL, 0.10 mmol) was carefully layered on top of an aqueous solution (1 mL) of metal nitrate hexahydrate salt (0.05 mmol) separated by a layer of DMF (0.5 mL).
Data for **1**: $Co(NO_3)_2·6H_2O$ (15.5 mg, 0.05 mmol). Pink crystals were harvested after a week. Yield 28 mg (74%). Found: C, 51.01; H, 6.57; N, 12.00. $[Co(H\mathbf{L})_2(H_2O)_4]·2DMF$ ($C_{30}H_{44}CoN_6O_{10}$) requires C, 50.92; H, 6.26; N, 11.87.
Data for **2**: $Ni(NO_3)_2·6H_2O$ (14.1 mg, 0.05 mmol). Small, pale blue crystals were harvested after a week. Yield 29 mg (87%). Found: C, 50.76; H, 6.50; N, 11.94. $[Ni(H\mathbf{L})_2(H_2O)_4]·2DMF$ ($C_{30}H_{44}NiN_6O_{10}$) requires C, 50.92; H, 6.26; N, 11.87.
Data for **3**: $Zn(NO_3)_2·6H_2O$ (16 mg, 0.05 mmol). Large, dull crystals were harvested after 1.5 weeks. Yield 17 mg.

Synthesis of {[Zn(HL)$_2$]·2CH$_3$OH·H$_2$O}, 4

H_2**L** (40.7 mg; 0.19 mmol) and $ZnSO_4·7H_2O$ (13.4 mg; 0.05 mmol) were heated in methanol (4 mL) in an ACE glass pressure tube at 80 °C for 48 h and then cooled slowly to room temperature. The reaction solution was replaced with fresh MeOH and the crystals were kept under solvent until analysis. A sample was dried under dynamic vacuum at 100 °C before microanalysis. Yield 9 mg (38 %). Found C, 57.14; H, 4.71; N, 11.14; $Zn(H\mathbf{L})_2·0.5H_2O$ ($C_{24}H_{24}N_4O_{4.5}Zn$) requires C, 57.10; H, 4.59; N, 11.10.

Synthesis of [Co(HL)$_2$], 5

H_2**L** (50 mg; 0.23 mmol) and $CoSO_4·7H_2O$ (100 mg; 36 mmol) were added to water (5 mL) in a Teflon lined Parr vessel and heated to 180 °C for 54 h and then cooled slowly to room temperature. The contents were a mixture of purple and colourless crystals. The majority of the colourless crystals of H_2**L** could be removed by swirling and decanting with portions of water. The remaining purple crystals were cleaned by short bursts of sonication with fresh portions of water. The crystals could also be cleaned by filtration and washing with DMF. Yield 44 mg (78 %). Found C, 58.5; H, 4.55; N, 11.3; $Co(H\mathbf{L})_2$ ($C_{24}H_{22}N_4O_4Co$) requires C, 58.9; H, 4.53; N, 11.5.

Synthesis of {[Cd(HL)$_2$(MeOH)$_2$]·1.8MeOH}, 6

A dilute solution of 2,6-lutidine in MeOH was diffused into a solution of H_2**L** (21.6 mg, 0.10 mmol) and $Cd(NO_3)_2·4H_2O$ (31 mg, 0.1 mmol) in MeOH (2 mL). This solution was filtered after 2 weeks and again after 4 weeks to remove small amounts of precipitated solid. After this time large polyhedral crystals grew over the course of the next 8 weeks. Yield 13 mg (47%) (after drying under dynamic vacuum at 100 °C). Found: C, 47.57; H, 5.00; N, 9.13. $[Cd(H\mathbf{L})_2(H_2O)_2]·1.5H_2O$ ($C_{24}H_{29}CdN_4O_{7.5}$) requires C, 47.58; H, 4.82; N, 9.24.

Synthesis of [Cu$_3$(HL)$_4$(μ$_2$-SO$_4$)(H$_2$O)$_3$]∞, 7; and {[Cu(HL)$_2$]·4CH$_3$OH·H$_2$O}∞, 8

$CuSO_4·5H_2O$ (31.7 mg, 0.127 mmol) was dissolved in methanol (3 mL) and added to a methanolic solution (13 mL) of H_2**L** (109.8 mg, 0.508 mmol). Under these conditions, crystals of coordination network **7** could be isolated after a few hours. If the solution was left to stand for a longer period, crystals of **7** transformed into **8** as small flower-like structures. The sample for elemental analysis was air dried over 13 days. Yield of **8**: 45 mg (69 %). Found: C, 55.49; H, 4.65; N, 10.77. $[Cu(H\mathbf{L})_2]·1.5H_2O$ ($C_{24}H_{25}CuN_4O_{5.5}$) requires C, 55.33; H, 4.84; N, 10.75.

Results and discussion

Synthesis and structural characterisation of H_2L and [H_3L]NO_3

Colourless crystals of H_2**L** were obtained during the synthesis of **5** (*vide infra*) and were analysed by single crystal X-ray diffraction. The structure was solved and refined in the triclinic space group *P*-1 with four unique molecules of the ligand in the asymmetric unit (Figure 2a). The essential differences between each molecule of H_2**L** resides in the pyrazole-phenyl torsion angles, which fall in the range 28.86(9) – 38.29(9) °.

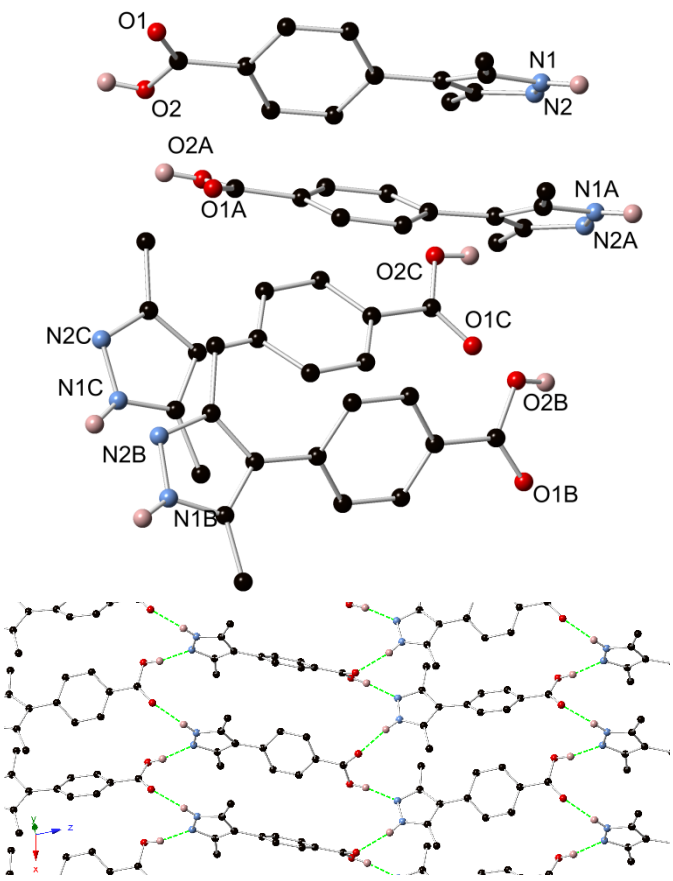

Figure 2 (a) Contents of the asymmetric unit of H_2**L** with heteroatoms labelled and selected hydrogen atoms shown; (b) Perspective view of the sheet structure formed in the *ac* plane by N-H···O and O-H···N hydrogen bonds, C-H hydrogen atoms omitted for clarity.

H_2**L** is replete with hydrogen bond donor and acceptor sites and O-H···N and N-H···O hydrogen bonds form between pyrazolyl and carboxylic acid functionalities in the crystal lattice. This takes the form of helical chains of hydrogen bonds running along the crystallographic *a*-axis which alternate handedness along the *c*-direction as ligands link chains into a 2D sheet in the crystallographic *ac* plane (Figure 2b). The X-ray structure determination confirms no prototropic tautomerism exists in neutral H_2**L**, which is in line with previous solid state ^{1}H NMR measurements.[30] Within each sheet, the phenyl rings of adjacent ligands which propagate along *a*-axis are offset, and this permits edge-to-face C-H···π interactions between adjacent phenyl groups to occur. No significant intermolecular interactions were observed between the 2D sheets, most likely due to the alternating twists of the phenyl rings preventing inter-sheet π-π stacking interactions.

The crystal structure of $[H_3$**L**$]NO_3$ (H_2**L**·HNO_3) was also determined. This salt formed in several attempted synthesis of coordination materials with metal nitrate salts; however, single crystals were prepared in a dedicated synthesis by heating a sample of H_2**L** in dilute nitric acid under hydrothermal conditions, followed by slow cooling. The asymmetric unit contains a nitrate anion and one cationic molecule (H_3**L**$^+$) featuring a pyrazolium ring, in the triclinic space group *P*-1 (Figure 3a). The pyrazolium moieties and nitrate anions associate *via* N-H···O hydrogen bonding about inversion centres such that nitrate anions bridge pyrazolium units in a ring structure $R_4^4(14)$ (Figure 3b). Carboxylic acid groups associate *via* hydrogen bonding to the equivalent site on another molecule in an $R_2^2(8)$ fashion typical of carboxylic acid dimers. The net result of these interactions is the formation of a 1-dimensional hydrogen-bonded tape, which propagates parallel to the [2,1,1] vector within the crystal lattice (Figure 3b). The alignment of dimeric units in $[H_3$**L**$]NO_3$ can be described as being head-to-head and tail-to-tail and is in contrast to the analogous structure of the trifluoroacetate salt which aligns in a 1D polymeric trifluoroacetate-bridged head-to-tail manner.[30] The polymer strands in $[H_3$**L**$]NO_3$ align in a staggered formation with equivalent units above and below each other and face-to-face π-π interactions between aligned pyrazole rings (average interplanar separation 3.302(2) Å) result in the formation of a sheet-like structure.

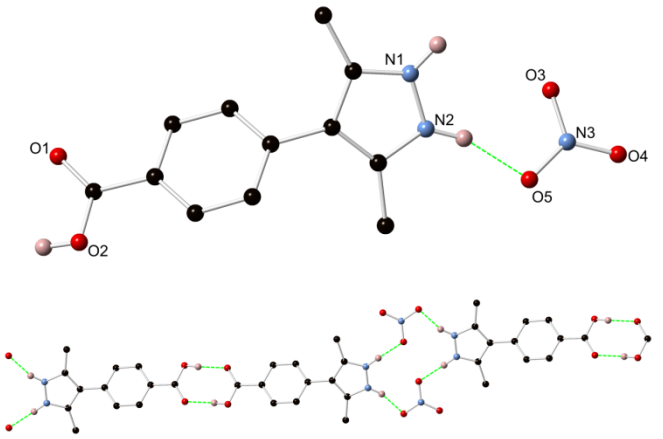

Figure 3 (a) The asymmetric unit of $[H_3$**L**$]NO_3$ with selected hydrogen atoms shown; (b) Part of the 1D polymeric structure of $[H_3$**L**$]NO_3$ showing the two hydrogen-bonding ring systems in the structure, C-H hydrogen atoms omitted for clarity.

Synthesis and structural characterisation of 1-8

Crystal structures of 1 and 2

Pink coloured crystals suitable for analysis by single crystal X-ray diffraction formed when the sodium salt Na[H**L**], prepared by the addition of one equivalent of 1 M aqueous sodium hydroxide to H_2**L** dissolved in DMF, was layered upon an aqueous solution of cobalt nitrate. The structure of **1** crystallises in the space group $P2_1/c$ with the asymmetric unit comprising of a cobalt atom located on a crystallographic inversion centre coordinated to one ligand via the N2 atom of the pyrazolyl ring and to two water molecules. Also in the asymmetric unit is a solvate DMF molecule. The pyrazolyl ring is neutral, and the H atom of the pyrazolyl ring could be located from Fourier residuals in the crystallographic refinement. To achieve charge balance, the ligand exists in a deprotonated carboxylate form

resulting in a HL^- binding mode. Thus, the structure exists as discrete molecular complexes (Figure 4a) with DMF solvate molecules in the lattice, with the formula $\{[Co(HL)_2(OH_2)_4]\cdot 2DMF\}$, **1**.

The discrete complexes arrange into a 3D hydrogen bonded polymeric structure through hydrogen bonds from coordinated pyrazolyl and water molecules to carboxylate groups of other complexes. The DMF guest interacts with an aqua ligand (C=O···H4A, 1.726 Å) and this ligand also acts with an adjacent pyrazolyl ring of the coordination sphere to cooperatively bind a carboxylate oxygen (O1′) from another complex (O1′···H4B, 1.83 Å, NH1···O1′ 1.92 Å, NH1···O1′···H4B, 72°). The other unique aqua ligand makes a hydrogen bond to the other carboxylate oxygen atom (O2′) of the nearby complex (O2′···H3B, 1.80 Å) fixing this into position in the network, as shown in Figure 4b. Extension of this motif reveals a hydrogen bonded rectangular 2D sheet. The result of the hydrogen-bonding pattern is to position carboxylate groups closely aligned to metal centres of other complexes in the sheets. A 3D hydrogen bonded superstructure is assembled when H3A interacts with the next sheet (O2″···H3A, 1.933 Å). The supramolecular structure is organised along the crystallographic *a*-axis into rectangular channels, in which the DMF guests are positioned (Figure 4b). The bulk purity of **1** was established through powder X-ray diffraction (PXRD) (Figure S2, ESI) and elemental analysis. Pale blue crystals of $\{[Ni(HL)_2(OH_2)_4]\cdot 2DMF\}$ **2** formed under the same reaction conditions using nickel(II) nitrate and were shown to be isostructural with **1** by PXRD (Figure S2, ESI).

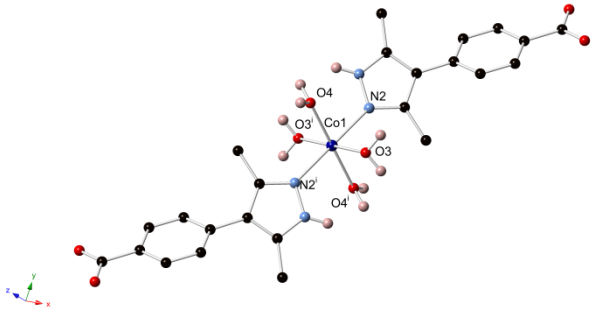

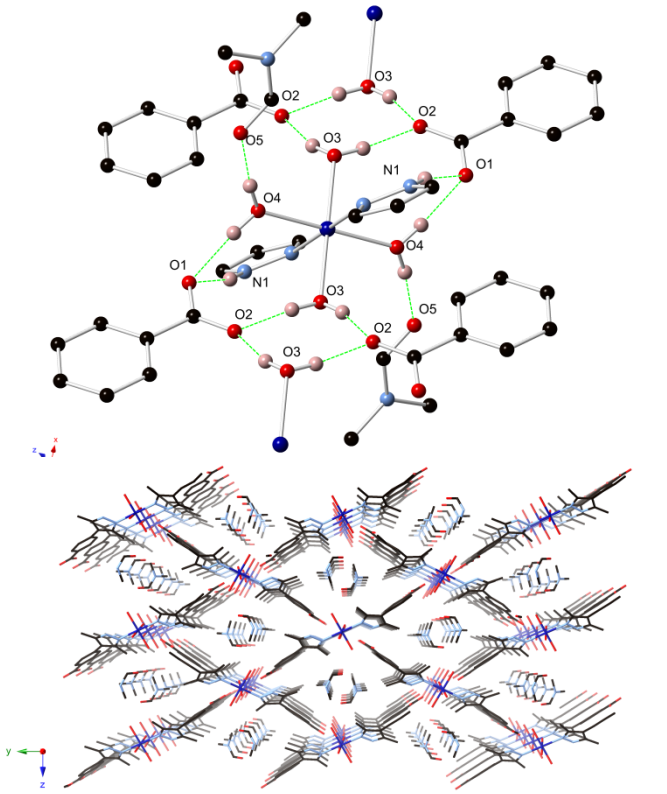

Figure 4 (a) The structure of the complexes in **1** with only selected hydrogen atoms shown; (b) A perspective view of the hydrogen bonding around the metal centres in **1**; (c) A view down the *a*-axis of the rectangular channels containing DMF guests in **1** with hydrogen atoms omitted for clarity. Symmetry codes used to generate equivalent atoms: (i) *–x*, *–y*, 2 – *z*.

Crystal structures of 3 and 4

The reaction of H_2L with zinc nitrate at room temperature under the same layering conditions in DMF, aqueous sodium hydroxide and water, followed a different course. Initially a powder formed and deposited and then large dull colourless crystals grew. These crystals proved suitable for structural analysis by X-ray diffraction. The structure crystallises in the space group *Fdd*2 with two unique zinc atoms lying on rotation axes that each coordinate HL^- ligands, a zinc atom lying on a 2-fold screw axis that coordinates two HL^- ligands via pyrazolyl N2 atoms, and a non-coordinating water molecule in the asymmetric unit. Each of the zinc atoms coordinates two pyrazolyl N2 atoms and two carboxyl O atoms, resulting in mixed N_2O_2 donor sets in distorted tetrahedral geometries (Figure 5a). Hydrogen bonding interactions between pyrazolyl N1H and the uncoordinated carboxyl oxygen atoms (N-H···O) exist around the coordination spheres of all zinc centres. The topology of the networks can be described as being distorted diamondoid (**dia**) with each zinc centre being a tetrahedral node and the bridging ligand acting as a linear link. Each network features large cavities with windows of *ca.* 20 × 30 Å and the material is quadruply interpenetrated (Figure 5b-c). Despite the high level of interpenetration, a PLATON analysis suggests

there are potential solvent accessible voids in the structure (25.1 % void volume). The electron density within these voids is diffuse and no ordered solvent molecules could be modelled crystallographically.

The PXRD patterns of crystals isolated and cleaned by sonication contain additional peaks when compared to the pattern simulated from the crystal structure analysis (Figure S4, ESI). The PXRD pattern for the powder that is formed initially could be recorded and matched well to the additional peaks seen in the pattern obtained from the crystals. Given the cleaning process and the relative intensities of the peaks due to each phase in the PXRD patterns of the crystals, the large crystals contain high proportions of both phases. Interestingly, the PXRD pattern of the powder was found to not match any structures previously reported for zinc coordination networks made from H_2**L**.

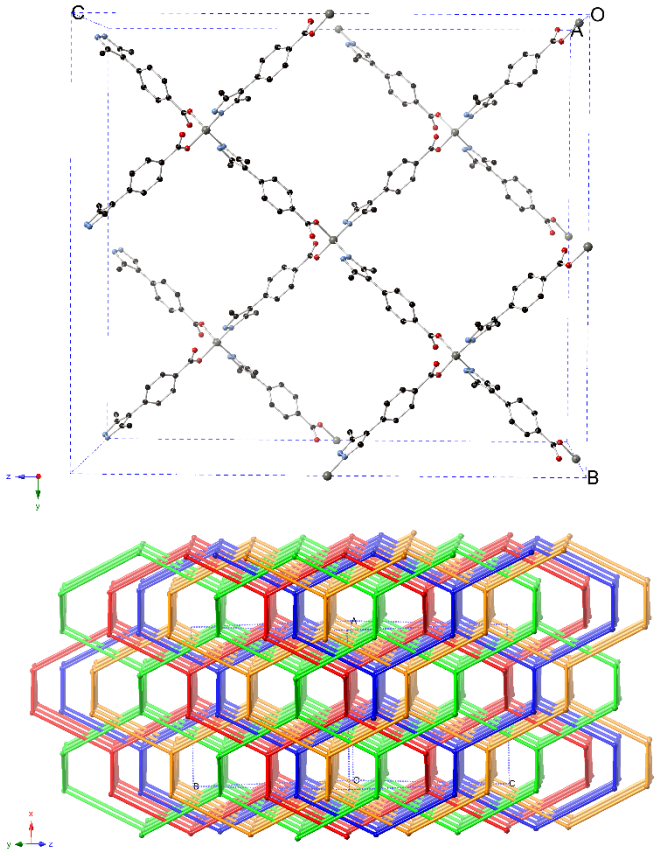

Figure 5 (a) Structure of a single network of **3/4** within the unit cell boundaries. Hydrogen atoms, interpenetrating networks and solvent molecules omitted for clarity. (b) Topological representation of the extended structure of **3/4**, independent networks coloured differently.

Changing the synthetic procedure to react H_2**L** with zinc sulfate in methanol at 80 °C yielded small well-formed colourless crystals suitable for structural analysis. The structure crystallises in the *Fdd*2 space group and is isostructural to the network described above. In the structural analysis of these crystals, however, the guest solvate molecules could be located and the full formula for this coordination network is $\{[Zn(HL)_2]\cdot 2CH_3OH\cdot H_2O\}_\infty$ **4**. This synthetic method gives a phase-pure zinc coordination polymer as judged by the excellent match between simulated and experimental PXRD patterns (Figure S5, ESI). The framework backbones of **3** and **4** are identical to that reported by Zhang who used different synthetic conditions of zinc nitrate in ethanol/water/DMA. The essential difference between the structures lies in the well-ordered methanol and water guests in coordination network **4** reported here.

Crystal structure of 5

To generate coordination networks with cobalt we explored reaction conditions at higher temperatures. The coordination polymer $[Co(HL)_2]_\infty$ **5** formed when H_2**L** and cobalt sulfate were reacted under hydrothermal conditions at 180 °C, with slow cooling to room temperature. A good yield of purple crystals was obtained (78%) after separation from crystallised H_2**L** by repeated decanting or by dissolution of unreacted H_2**L** in DMF and filtration. The purple crystals were subjected to a single crystal X-ray diffraction study, and the data was solved and refined in the tetragonal space group *I*-42*d*. The model determined for the asymmetric unit is comprised of two crystallographically unique Co(II) ions laying on rotoinversion axes that are each coordinated to a unique molecule of HL^-. As such, each Co(II) coordinates to four crystallographically equivalent ligand molecules in a tetrahedral fashion with a mixed N_2O_2 donor set (Figure 6a). These structural units are unique due to differences in angles about the coordination spheres of the cobalt atoms, and the torsion angles between pyrazole and phenyl rings of the ligands.

In the same manner as **3** and **4**, N-H···O hydrogen bonding between pyrazolyl N1H and carboxyl groups is present around the cobalt coordination spheres in **5**, as shown in Figure 6a, and when each crystallographically unique unit is extended into three dimensions, distorted **dia** networks are observed. The material is also quadruply interpenetrated (Figure 6b) and **5** can be viewed as consisting of two sets of two crystallographically equivalent networks. In contrast to **3** and **4**, the networks pack closely and **5** contains no void space. This coordination network is similar to that described by Zhang et al{He, 2014 #543} for a nonporous zinc network of HL^- synthesised under hydrothermal conditions.

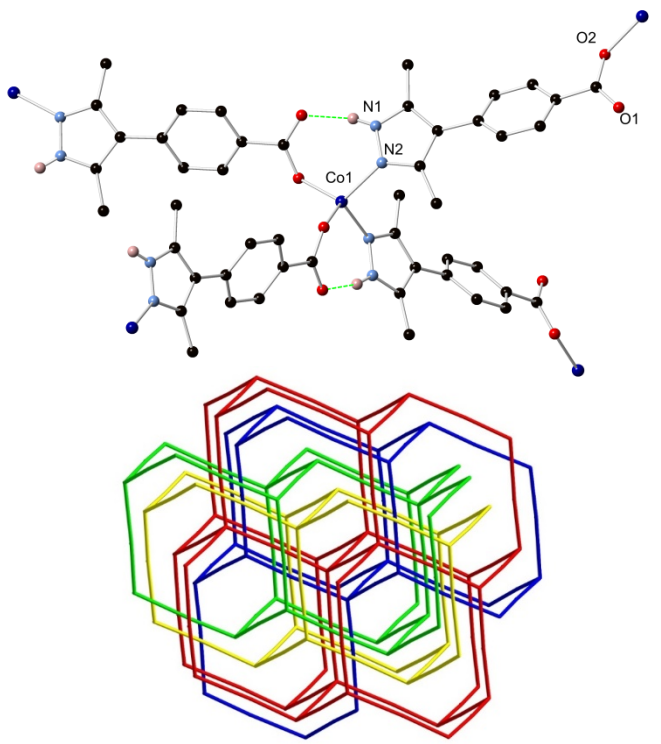

Figure 6 (a) The structure of one of the metal nodes in the structure of **5** with selected hydrogen atoms shown to highlight the hydrogen bonding around the coordination sphere; (b) Perspective view of the quadruply interpenetrating nets in 5. Symmetry related nets are red-blue and green-yellow.

Crystal structure of 6

Large polyhedral crystals of {[Cd(H**L**)$_2$(MeOH)$_2$]·1.8MeOH} **6** formed over a period of several weeks when 2,6-dimethylpyridine was diffused at room temperature into a methanol solution of H$_2$**L** and cadmium nitrate. The coordination network crystallises in the space group *C*2/*c* with a Cd centre, located on a crystallographic 2-fold rotation axis, coordinating a ligand of H**L**$^-$ and a methanol ligand in the asymmetric unit. The hydrogen atom of the hydroxyl group in the ligated methanol was readily located and was refined at a distance of 0.95 Å from O3. The asymmetric unit is completed with disordered and partially occupied guest molecules that were modelled with restraints and without hydrogen atoms as methanol.

The cadmium(II) centre is 6-coordinate with a highly distorted octahedral geometry. The methanol ligands coordinate in a *trans* orientation (166.9°) and the equatorial plane consists of a N_2O_2 set of donors from H**L**$^-$ ligands configured in a *cis* geometry around the equatorial plane (N2···Cd···N2′, 97.7°; N2···Cd···O2′, 90.2°; O2···Cd···O2′, 86.7°). Hydrogen bonding between pyrazolyl N1H and carboxyl oxygen atom O1 (N1H···O1, 2.05 Å) is present around the cadmium coordination spheres in **6**, as shown in Figure 7a. The network assembles into a (4,4)-sheet in the crystallographic *ab*-plane. The coordination angles between H**L**$^-$ ligands subtended at the metal centres create rhomboidal solvent channels in the sheets. Sheets stack in the *c*-direction through hydrogen bonds from the hydroxyl groups of axial methanol ligands to uncoordinated carboxyl oxygen atoms of H**L**$^-$ (O1) in the next layer (O-H···O=C, 1.74 Å) and so the rhomboidal pore shape is extended into 1D channels in the structure, within which the methanol guests are located.

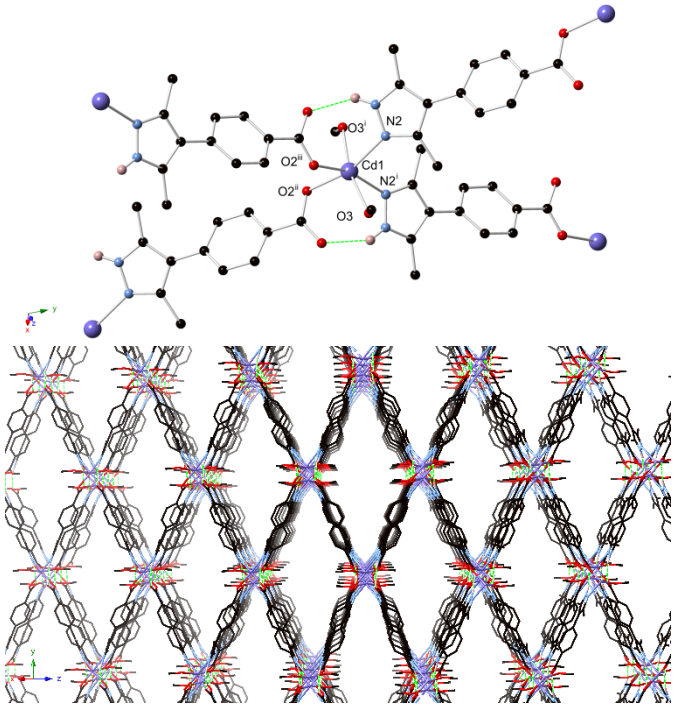

Figure 7 (a) A view of the a metal node in the structure of **6** with selected hydrogen atoms shown to highlight the hydrogen bonding around the coordination sphere; (b) A view down the 1D channels along the *c*-axis in the structure of **6** with hydrogen atoms and guest solvent molecules removed for clarity. Symmetry codes used to generate equivalent atoms: (i) $1-x, +y, {}^1/_2-z$; (ii) ${}^1/_2+x, {}^1/_2+y, +z$; (iii) ${}^3/_2-x, {}^1/_2+y, {}^1/_2-z$.

Crystal structures of 7 and 8

The reaction of H$_2$**L** with copper(II) sulfate was first carried out in a 2:1 ligand to metal ratio in methanol solution at room temperature. Pale green plate crystals formed after several hours and this green phase transformed to purple crystals over time. Modifying the preparation conditions to a 4:1 ligand to metal ratio sometimes saw the formation of the green crystals but more often resulted only in the purple phase appearing. The green crystals were subjected to single crystal X-ray diffraction using synchrotron radiation. The small size and quality of individual crystallites and possibly the metastable nature of the crystals contributed to poor diffraction and a low resolution structure solution was obtained in the monoclinic space group *C*2/*m*. The asymmetric unit contains three crystallographically unique copper sites, each with coordinated water molecules; Cu1 also coordinates a sulfate anion and the asymmetric unit is completed by two H**L**$^-$ ligands that bridge the three copper(II) ions, resulting in a formula for the network of $[Cu_3(HL)_4(SO_4)(OH_2)_3]_\infty$ **7**. Intriguingly, there are two types of metal node in **7** that display conserved binding domains of the

ligand. Cu1 exhibits five coordinate geometry that is distorted from square pyramidal, if one considers Cu1 to coordinate to two pyrazole N2 atoms, an aqua ligand, and an oxygen atom of the sulfate anion, in the basal plane. The apical site is occupied by another sulfate oxygen atom related by crystallographic symmetry. The sulfate anions engage in a μ_2-O mode bridging crystallographically equivalent copper ions about a centre of inversion into a dicopper unit. This unit is supported by four hydrogen-bonding interactions between pyrazolyl donors and non-coordinating sulfate oxygen atom O4 and O6 acceptors (N1H···O-S), two of which are shown in Figure 8a. Copper ions Cu2 and Cu3 each adopt square pyramidal coordination geometry within different dicopper paddlewheel clusters, through coordination to carboxylate oxygen atoms of H**L**$^-$ and axial aqua ligands. Each paddlewheel unit is comprised of only one crystallographically unique copper atom and carboxylate group. This conserved coordination arrangement is an example of the potential afforded by heteroditopic ligands to assemble in this way and create complex structures. The two molecules of H**L**$^-$ within the asymmetric unit are geometrically related by non-crystallographic mirror symmetry through the Cu1-O3-Cu1(i) plane, however, the lattice symmetry prevents crystallographic equivalence.

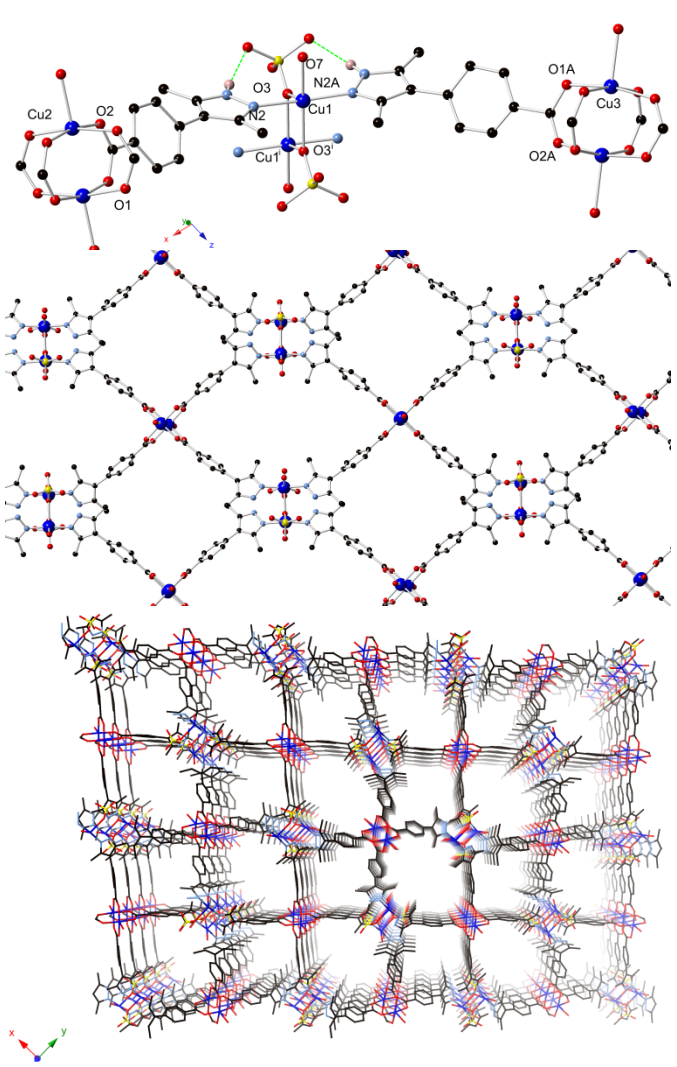

Figure 8 (a) A view showing the two types of node in the structure of **7**. Selected hydrogen atoms are shown to highlight the hydrogen bonding around the dicopper-pyrazolyl node; (b) The extension of the structure into a 2D sheet with the hydrogen atoms removed for clarity; (c) A view of the solvent channels that exist along the *c*-axis in the structure of **7,** hydrogen atoms are removed for clarity. Symmetry codes used to generate equivalent atoms: (i) $^1/_2 - x, ^1/_2 - y, -z$.

Extension of **7** through the two types of dicopper clusters results in the formation of a (4,4) two-dimensional network, in which the Cu_2 paddlewheel and $Cu_2(OSO_3)_2$ clusters both act as four-connected nodes, bridged through linear H**L**$^-$ links (Figure 8b). The stacking of the sheets gives rise to two types of 1D channels running parallel to the crystallographic *c*-axis, as shown in Figure 8c. The channels make up 42% of the unit cell volume but the low quality of the diffraction data, and the diffuse nature of the residual Fourier difference peaks within these channels, meant the contents of the channels were not able to be modelled and the SQUEEZE routine within PLATON was applied to the data in order to provide more meaningful refinement statistics.

The purple crystals **8** were of good quality and were analysed by single crystal X-ray diffraction. The material crystallises in the tetragonal space group $I4_1/a$ with the

asymmetric unit containing a half-occupancy copper atom residing on an inversion centre that is coordinated to a H**L**$^-$ ligand. The asymmetric unit is completed by a well-ordered methanol guest molecule, and a second methanol guest molecule disordered in a 57:43 ratio, as well as a half occupancy guest water molecule. This gives the coordination network **8** a formula of $\{[Cu(H\mathbf{L})_2]\cdot 4CH_3OH\cdot H_2O\}_\infty$. By virtue of the inversion centre, the angles between equivalent coordinating atoms about the copper coordination sphere are 180° and the unique O-Cu1-N angles are 88.07(9)° and 91.93(9)° in the square-planar geometry. The hydrogen-bonding interactions that are present around the metal coordination spheres in other networks consisting of a single metal node are not present here. Instead, there are hydrogen bonds made from pyrazolyl NH1 to the disordered site of the methanol guests (NH···O), and the well-ordered methanol guest makes a hydrogen bond to the uncoordinated oxygen of the ligand carboxyl group (O-H···O=C, 2.086 Å).

The structure expands through the 4-connected square planar nodes and linear linking ligands into the **lvt** network. The network has large windows when viewed along the *a* or *b*-axis of 25 × 35 Å (Figure 9b). This network is interpenetrated by two other networks and therefore **8** is a triply interpenetrated coordination material. Small pores exist in the material and contain the water and methanol guests.

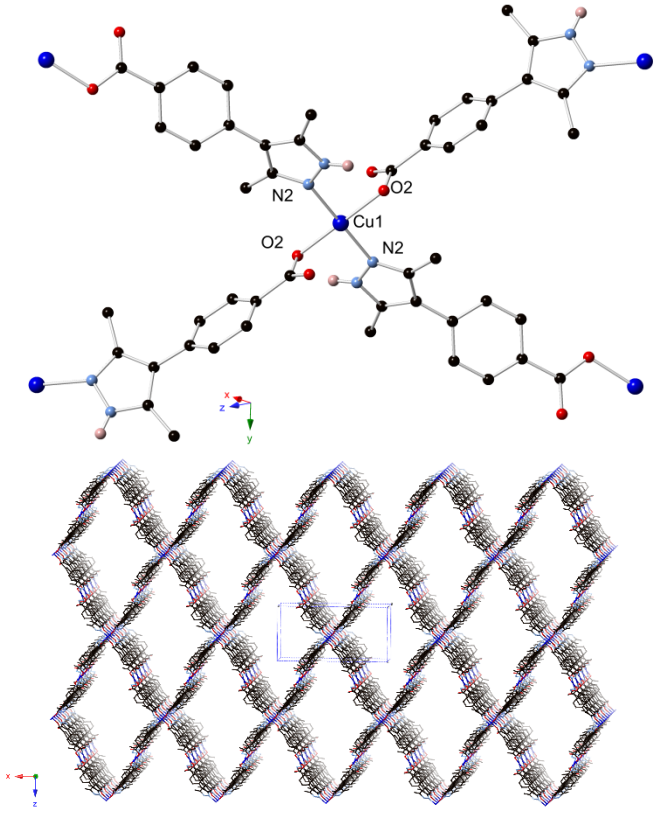

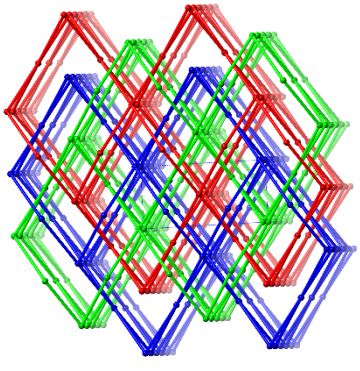

Figure 9 (a) A view of the metal node in the structure of **8**; (b) A view of the large channels that form in a single network of **8** with hydrogen atoms and guest solvent molecules removed for clarity; (c) a perspective of the network catenation present in **8**. Symmetry codes used to generate equivalent atoms: 1 – *x*, 1 – *y*, 1 – *z*.

Crystals of **8** visually appeared to retain single crystallinity after removal from methanol solution and drying and this encouraged us to collect single crystal diffraction data on dried crystals (**8**-*dry*). The diffraction experiments revealed high mosaicity perhaps caused by cracking of the crystals during desolvation and a low resolution structure model could be obtained in the monoclinic space group *I*2/*a* with the help of synchrotron radiation. The structure of the asymmetric unit of **8**-*dry* retains the same connectivity to that seen in **8**; that is, Cu(II) ions coordinating to two pyrazole and two carboxylate groups from anionic H**L**$^-$ ligands around a square planar arrangement. This arrangement means the topology of the **lvt** network observed in the fully solvated network of **8** is retained. The structure was modelled with two Cu(II) ions disordered over two positions each, and two unique molecules of H**L**$^-$ in the asymmetric unit, each of which have extensive disorder around both coordinating sites and torsional disorder between the pyrazole and phenyl rings. The structure model was examined closely for residual electron density. As shown in Figure 10, electron density was detected in the vicinity of the axial positions of the metal ions, which might indicate the partial coordination of water to these sites during the desolvation process, and there are other areas of electron density in the restricted pore spaces in the material. With the X-ray data quality severely restricted by poor crystallinity further interpretation of the structure model is not justified and we sought to obtain supporting information regarding the desolvation process through a range of other techniques.

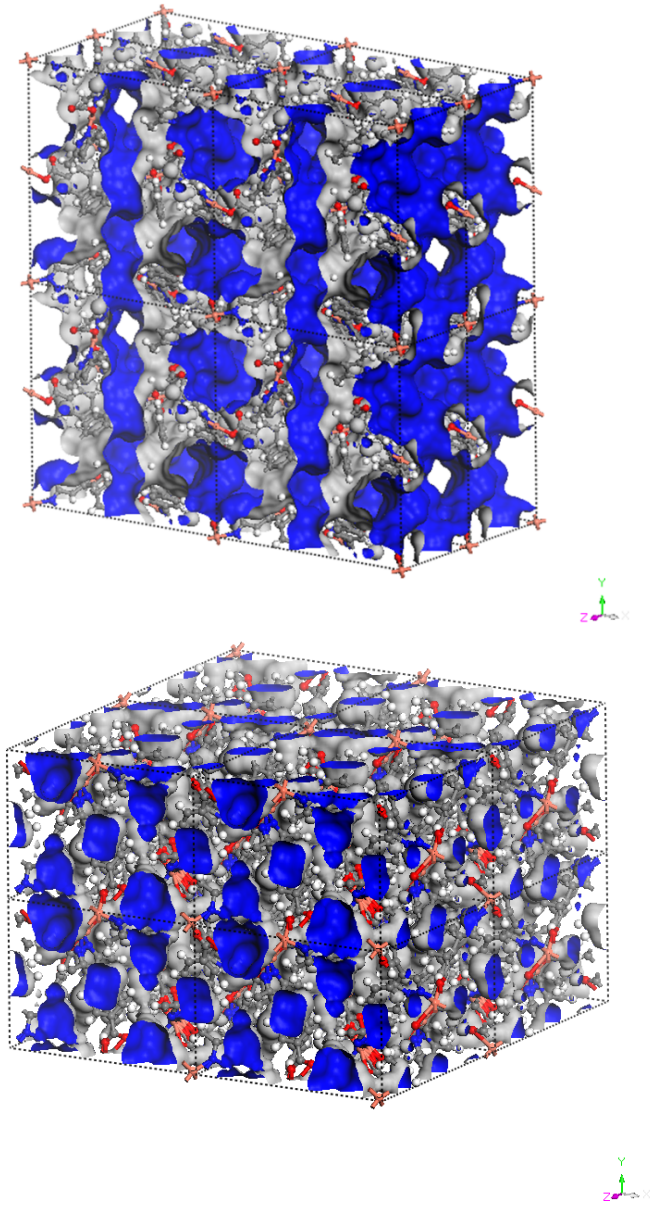

Figure 10 Perspective views of Connelly surfaces of 2 × 2 × 2 unit cells of **8** (top) and **8**-*dry* (bottom) with solvate molecules removed to highlight the channels that exist in **8** and small solvent accessible areas in **8**-*dry*.

Powder X-ray diffraction (PXRD) was used to follow the changes when **8** was removed from solvent and allowed to air dry (Figure 11; Figure S10 ESI). The PXRD traces show changes to the peak positions indicating a structural transformation begins when the crystals are removed from methanol solution. Over the first 9 hours the low angle reflections at 7.5° and 10.5° move to slightly higher 2θ angles and then lose intensity. A new peak at 8.0° and peaks around 13.8° grow into the patterns but fall off in intensity around the 24 h mark. A phase with reasonable crystallinity is seen between 15-21 h and these peaks die away by the 24 h mark. The sample continues to change after 24 h with new broad peaks growing in to the pattern around 7°, between 12-13°, 15° and 20° in 2θ. These peaks are dominant in the patterns from 39 h onward. From these observations, it is clear that the desolvation process is complicated and we suspect **8** moves through at least one and perhaps more intermediate structures before the structural transformation is complete and this process takes around three days at room temperature.

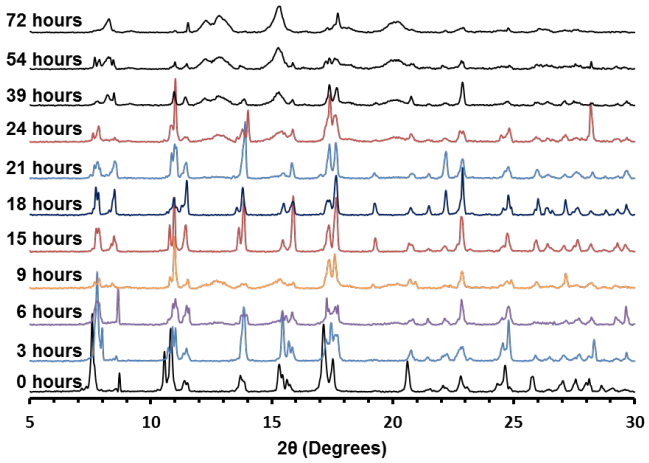

Figure 11 PXRD patterns taken at time points over 72 h following the removal of **8** from solvent.

IR spectroscopy (Figure S22, ESI) indicates the presence of water in air-dried samples and microanalysis confirms that 1.5 molecules of water per formula unit are present in the crystals after air drying. The impact of desolvation on the crystallinity was also studied by heating samples of **8** in a thermogravimetric analyser (a description of the full thermogravimetrogram is discussed later) with analysis by PXRD afterward. We observed that completely removing the methanol and water by heating gave PXRD traces that were reasonable matches compared to the pattern simulated from the single crystal analysis of **8**-*dry* (Figure S9, ESI). We also found that the structure did not take up any water once desolvated, indicating this materials response to complete guest loss is a considerable loss of crystallinity and closure of its pores.

Thermal Studies of 1-2, 4-6 and 8

Compounds **1-2**, **4-6** and **8** were studied by simultaneous thermogravimetric-differential thermal analysis (TG-DTA). The power of TG-DTA lies in its ability to identify energy changes that occur in the sample with no loss of mass, which TG analysis alone cannot identify.[31, 32] For example, we have used TG-DTA to identify molecular rearrangements in porous MOFs that are not accompanied by mass loss or a change of phase.[33, 34]

TG-DTA Study on 1 and 2

The TG-DT analysis of $[Co(H\mathbf{L})_2(OH_2)_4]\cdot 2DMF$ **1** is shown in Figure 11 (Figure S11, ESI). The mass loss between 100 and 200 °C is 30.8% and is consistent with the loss from the

crystals of the DMF guests and all water molecules bound to the cobalt centre (calc. 30.8%). The loss is endothermic in nature with the peak maximum for this process occurring at 133 °C. The desolvated structure is stable until 250 °C whereupon the sample begins to lose mass gradually and at 375 °C major breakdown of the material occurs in an exothermic process. The breakdown is complete at 520 °C with only 10.0% of the mass remaining, most likely as CoO (Calc. 10.5%). The TG analysis of $[Ni(HL)_2(OH_2)_4]\cdot 2DMF$ **2** is very similar with a 29.9% mass loss between 100 and 200 °C (calc. 30.8%) and major breakdown starting at 370 °C (Figure S12, ESI).

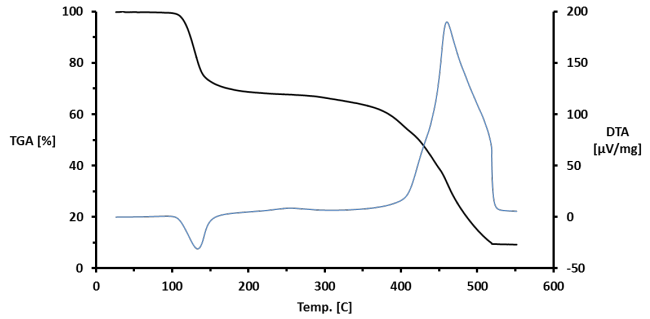

Figure 11 Thermogravimetric (black) and differential response (blue) curves for **1**

Having identified in **1** that aqua ligands position carboxylate groups proximal to the metal centres by hydrogen bonds, we wondered if dehydration of the metal centres would induce the close-by carboxylates to coordinate and thereby form a coordination network. Such a conversion has been achieved by the thermal treatment of a cadmium complex with a structurally related 1,2,4-triazolyl benzoate ligand.[35] Accordingly, **1** was heated until the DMF guests and aqua ligands were removed and a purple powder was recovered (**1**-*desolv*) and was analysed by PXRD. Although the PXRD pattern (Figure S3, ESI) showed very little crystallinity in the material, it is notable that when **1**-*desolv* was exposed to a solution of DMF and water that **1** was not regenerated and it seems likely that **1**-*desolv* is an amorphous coordination polymer with the formula $[Co(HL)_2]_\infty$.

TG-DTA Study on 4

Upon isolation, the crystals of **4** quickly lose solvent and turn opaque. This thwarted our attempts to record data on fully solvated samples. The TG-DTA recorded (Figure S13, ESI) shows a 5 % mass loss of remaining solvent coming from the structure under 50 °C, which is likely to be some remaining methanol (calc. loss for one methanol 5.5 %) and this is accompanied by a small endothermic signal in the DTA. The material continues to lose a further 5 % mass out to nearly 400 °C whereupon it undergoes rapid mass loss in exothermic decomposition steps. The decomposition is complete just after 500 °C with 11.5 % mass remaining, presumably as ZnO.

TG-DTA Study on 5

Consistent with the dense quadruply interpenetrated structure of $[Co(HL)_2]$ **5**, the TG curve (Figure S14, ESI) shows that only 1.8% of mass is lost from the sample up to 400 °C and there are no thermal events detected by DT analysis until the onset of decomposition. The decomposition is strongly exothermic and complete by 525 °C and the mass remaining above this temperature is likely to be CoO (obs. 14.9%; calc. 15.3%).

TG-DTA Study on 6

The extremely rapid loss of methanol from the pores of $[Cd(HL)_2(MeOH)_2]\cdot 1.8MeOH$ **6** prevented the capture of this information in our TG-DTA studies. The desolvated form, $[Cd(HL)_2(MeOH)_2]$ (**6**-*dry*), was studied and TG-DT analysis for **6**-*dry* is shown in Figure 12 (Figure S15, ESI). The bound methanol ligands are liberated from the metal centres in the network by 120 °C (obs. mass loss 10.4%; calc. 10.5%) and the DT curve shows this to be an endothermic process centred at 112 °C. There is little further loss in mass until 272 °C at which point the DT curve shows a clear exotherm. This seems to trigger the decomposition of **6**-*dry* with a further 7.5 % mass loss observed up to 400 °C and then large losses totalling 53 % mass up to 550 °C in two exothermic decomposition steps.

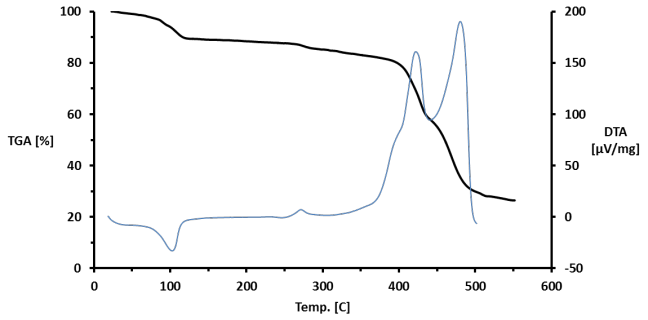

Figure 12 Thermogravimetric (black) and differential response (blue) curves for **6**-*dry*.

TG-DTA Study on 8

The TG-DT analysis for **8** supports the formulation of $\{[Cu(HL)_2]\cdot 4MeOH\cdot H_2O\}$ derived from the single crystal X-ray structure. The TG curve shows a mass loss of 19.2% up to 100 °C and a further 2.8% up to 150 °C, fully consistent with the loss of four methanol molecules (calc. 20.0%) and a water molecule (calc. 2.8%) (Figure 13, Figure S16, ESI). Matching peaks are found in the DT curve with peak maxima centred at 77 °C and 135 °C, respectively. The temperature of 135 °C for the removal of water from the pore structure indicates the strong affinity that water has for the framework and this is a reflection of the position that water occupies in the structure. The sample mass plateaus until an exotherm is observed in the DT curve at 222 °C. The sample begins to lose mass after this point with a further 5% lost up to 320 °C and above this temperature there is rapid onset of exothermic decomposition until only CuO remains by 445 °C (obs. 10.4%; calc. 10.3%).

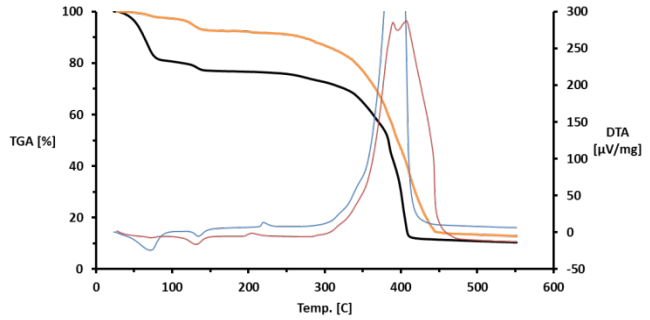

Figure 13 Thermogravimetric (black) and differential response (blue) curves for as synthesised **8**; Thermogravimetric (orange) and differential response (red) curves for air-dried **8**.

Upon standing **8** in air for a day the methanol from the pore structure is nearly all lost. The TG analysis curve shows a 2.7% mass loss up to 100 °C, corresponding to half a remaining methanol per Cu(H**L**)$_2$ formula unit (calc 2.8%), and a further 4.3% mass loss to 150 °C that accounts for 1.5 water molecules (calc. 4.3%). The change in the populations of framework guests is reflected in the corresponding DT peaks. The peak centred at 75 °C is very broad and low in intensity while the DT peak at 135 °C has become more intense. Microanalysis on air dried material confirms that there remains 1.5 guest water molecules per formula unit, [Cu(H**L**)$_2$]·1.5H$_2$O, consistent with the electron density observed in the crystal structure of the desolvated material.

Conclusions

A variety of structure types were observed in this work, including discrete coordination complexes arranged by multiple hydrogen bonds into 3D superstructures, 2D sheet structures assembled in the third dimension by inter-sheet hydrogen bonds and a number of highly interpenetrated 3D coordination networks. The highly interpenetrated structures **3**-**5** and **8** contain single metal ion nodes and it is likely that these small nodes contribute to the highly interpenetrated structures observed. The zinc coordination networks **3** and **4** are isostructural and form the **dia** structure type under very different synthetic conditions, indicating the strong preference for this structure over others. This result adds to the work reported by Zhang on different inclusion isomers of this network.[18]

A significant feature of the metal ion nodes in all the structures is the interplay of hydrogen and coordinate bonding around the coordination spheres, specifically NH···O hydrogen bonding between coordinated pyrazole and carboxylate. The ligand bridges metal centres in the coordination networks in the anionic H**L**$^-$ form, wherein the carboxylate carries the negative charge and the pyrazole ring retains its hydrogen atom and is neutral. The use of the weakly basic nitrate and sulfate counter ions in the syntheses and, in general, mild reaction conditions seem to favour this mode of bonding. The anionic nature of the ligand gives rise to neutral coordination networks and coordination complexes **1** and **2**.

The most prevalent donor set observed is N_2O_2 on single metal ion nodes in tetrahedral or square planar configurations. This node type is often seen in coordination networks derived from co-ligand systems such as bridging dicarboxylates and diazoles.[36, 37] The exception to this is seen in coordination network **7** where conserved binding domains of the ligand are observed in different dicopper aggregates. This structure is meta-stable and intercepted *en route* to a thermodynamically stable phase containing single metal ion nodes with N_2O_2 donor sets. This highlights, perhaps, the intrinsic difficulty in using heteroditopic ligands to engineer coordination networks featuring nodes with conserved binding domains.

Acknowledgements

CR gratefully acknowledges support from the University of Wollongong for this research. CSH and PEK gratefully acknowledge the University of Canterbury (College of Science scholarship to CSH) and the Royal Society of New Zealand Marsden Fund for financial support. Parts of this work were carried out on the MX1 Macromolecular Crystallography beam line at the Australian Synchrotron, Victoria, Australia. ADB gratefully acknowledges the EPSRC and the University of Bath for financial support.

Notes and references

[a] *School of Chemistry, Faculty of Science, Medicine and Health, University of Wollongong, Wollongong NSW 2522, Australia; Fax: +61 2 4221 4287; Tel:+ 61 2 4221 3254; E-mail: chris_richardson@uow.edu.au*
[b] *Department of Chemistry, University of Bath, Claverton Down, Bath BA2 7AY, UK; E-mail: a.d.burrows@bath.ac.uk*
[c] *Department of Chemistry, University of Canterbury, Private Bag 4800, Christchurch 8140, New Zealand.*
[d] *MacDiarmid Institute for Advanced Materials and Nanotechnology, Department of Chemistry, University of Canterbury, Private Bag 4800, Christchurch 8140, New Zealand. E-mail: paul.kruger@canterbury.ac.nz*

Electronic Supplementary Information (ESI) available: synthetic details for the preparation of **H$_2$L**. PXRD patterns of **1**-**6**, **8**. Further TG-DTA traces for **H$_2$L**, **1**-**6**, **8**. Infrared spectra of **1**, **1**-*desolv*, **2**, **4**, **5**, **6**-*dry*, and air- and TGA-dried **8**. See DOI: 10.1039/b000000x/

1. S. R. Batten, S. M. Neville and D. R. Turner, *Coordination Polymers*, The Royal Society of Chemistry, 2009.
2. H.-C. Zhou, J. R. Long and O. M. Yaghi, *Chemical Reviews*, 2012, **112**, 673-674.
3. W. Lu, Z. Wei, Z.-Y. Gu, T.-F. Liu, J. Park, J. Park, J. Tian, M. Zhang, Q. Zhang, T. Gentle Iii, M. Bosch and H.-C. Zhou, *Chemical Society reviews*, 2014, **43**, 5561-5593.
4. A. D. Burrows, D. J. Kelly, M. I. Haja Mohideen, M. F. Mahon, V. M. Pop and C. Richardson, *CrystEngComm*, 2011, **13**, 1676.
5. C. S. Hawes and P. E. Kruger, *Aust. J. Chem.*, 2013, **66**, 401-408.
6. C. S. Hawes, R. Babarao, M. R. Hill, K. F. White, B. F. Abrahams and P. E. Kruger, *Chemical communications*, 2012, **48**, 11558-11560.
7. C. S. Hawes and P. E. Kruger, *Dalton Trans.*, 2014, **43**, 16450-16458.

8. C. S. Hawes, B. Moubaraki, K. S. Murray, P. E. Kruger, D. R. Turner and S. R. Batten, *Crystal Growth & Design*, 2014, 141009095854007.
9. V. Colombo, S. Galli, H. J. Choi, G. D. Han, A. Maspero, G. Palmisano, N. Masciocchi and J. R. Long, *Chemical Science*, 2011, **2**, 1311.
10. H. J. Choi, M. Dincă and J. R. Long, *Journal of the American Chemical Society*, 2008, **130**, 7848-7850.
11. E. Q. Procopio, N. M. Padial, N. Masciocchi, S. Galli, J. E. Oltra, E. Barea and J. A. R. Navarro, *CrystEngComm*, 2013, **15**, 9352-9355.
12. N. M. Padial, E. Quartapelle Procopio, C. Montoro, E. Lopez, J. E. Oltra, V. Colombo, A. Maspero, N. Masciocchi, S. Galli, I. Senkovska, S. Kaskel, E. Barea and J. A. Navarro, *Angewandte Chemie*, 2013, **52**, 8290-8294.
13. V. Colombo, C. Montoro, A. Maspero, G. Palmisano, N. Masciocchi, S. Galli, E. Barea and J. A. R. Navarro, *J. Am. Chem. Soc.*, 2012, **134**, 12830-12843.
14. E. Quartapelle Procopio, T. Fukushima, E. Barea, J. A. R. Navarro, S. Horike and S. Kitagawa, *Chem. - Eur. J.*, 2012, **18**, 13117-13125, S13117/13111-S13117/13117.
15. C. Montoro, F. Linares, E. Quartapelle Procopio, I. Senkovska, S. Kaskel, S. Galli, N. Masciocchi, E. Barea and J. A. R. Navarro, *J. Am. Chem. Soc.*, 2011, **133**, 11888-11891.
16. C. Heering, I. Boldog, V. Vasylyeva, J. Sanchiz and C. Janiak, *CrystEngComm*, 2013, **15**, 9757-9768.
17. C.-T. He, J.-Y. Tian, S.-Y. Liu, G. Ouyang, J.-P. Zhang and X.-M. Chen, *Chemical Science*, 2013, **4**, 351.
18. C.-T. He, P.-Q. Liao, D.-D. Zhou, B.-Y. Wang, W.-X. Zhang, J.-P. Zhang and X.-M. Chen, *Chemical Science*, 2014, **5**, 4755-4762.
19. A. Torres-Knoop, R. Krishna and D. Dubbeldam, *Angewandte Chemie International Edition*, 2014, **53**, 7774-7778.
20. Z. Wei, D. Yuan, X. Zhao, D. Sun and H.-C. Zhou, *Science China Chemistry*, 2013, **56**, 418-422.
21. W. M. Bloch, A. Burgun, C. J. Coghlan, R. Lee, M. L. Coote, C. J. Doonan and C. J. Sumby, *Nature chemistry*, 2014, **6**, 906-912.
22. W. M. Bloch, C. J. Doonan and C. J. Sumby, *CrystEngComm*, 2013, **15**, 9663.
23. T. M. McPhillips, S. E. McPhillips, H.-J. Chiu, A. E. Cohen, A. M. Deacon, P. J. Ellis, E. Garman, A. Gonzalez, N. K. Sauter, R. P. Phizackerly, S. M. Soltis and P. Kuhn, *J. Synchrotron Rad.*, 2002, 401-406.
24. W. J. Kabsch, *J. Appl. Cryst.*, 1993, 795-800.
25. S. Brennan and P. L. Cowan, *Rev. Sci. Instrum.*, 1992, **63**, 850-853.
26. G. M. Sheldrick, *Acta Crystallogr. Sect. A*, 2008, **64**, 112–122.
27. G. M. Sheldrick, *SHELXL-97, Programs for X-ray Crystal Structure Refinement;* , University of Göttingen, Germany, 1997.
28. O. V. Dolomanov, L. J. Bourhis, R. J. Gildea, J. A. K. Howard and H. Puschmann, *J. Appl. Cryst.*, 2009, **42**, 339-341.
29. L. J. Barbour, *J. Supramol. Chem.*, 2001, **1**, 189-191.
30. C. Foces-Foces, C. Cativiela, M. Zurbano, I. Sobrados, N. Jagerovic and J. Elguero, *J Chem Crystallogr*, 1996, **26**, 579-584.
31. J. J. Vittal, *Coordination Chemistry Reviews*, 2007, **251**, 1781-1795.
32. G. K. Kole and J. J. Vittal, *Chemical Society reviews*, 2013, **42**, 1755-1775.
33. A. D. Burrows, S. O. Hunter, M. F. Mahon and C. Richardson, *Chemical communications*, 2013, **49**, 990-992.
34. L. Tshering, S. O. Hunter, A. Nikolich, E. Minato, C. M. Fitchett, D. M. D'Alessandro and C. Richardson, *CrystEngComm*, 2014, **16**, 9158-9162.
35. D. Lässig, J. Lincke, R. Gerhardt and H. Krautscheid, *Inorganic chemistry*, 2012, **51**, 6180-6189.
36. A. Goswami, S. Sengupta and R. Mondal, *CrystEngComm*, 2012, **14**, 561-572.
37. R. Mondal, M. K. Bhunia and K. Dhara, *CrystEngComm*, 2008, **10**, 1167-1174.